Neuro-Oncology

Neuro-Oncology 18(1), 132–141, 2016
doi:10.1093/neuonc/nov147
Advance Access date 4 August 2015

Differentiation of high-grade and low-grade diffuse gliomas by intravoxel incoherent motion MR imaging

Osamu Togao, Akio Hiwatashi, Koji Yamashita, Kazufumi Kikuchi, Masahiro Mizoguchi, Koji Yoshimoto, Satoshi O. Suzuki, Toru Iwaki, Makoto Obara, Marc Van Cauteren, and Hiroshi Honda

Department of Clinical Radiology, Graduate School of Medical Science, Kyushu University, Fukuoka, Japan (O.T., A.H., K.Y., K.K., H.H.); Department of Neurosurgery, Graduate School of Medical Sciences, Kyushu University, Fukuoka, Japan (M.M., K.Y.); Department of Neuropathology, Graduate School of Medical Sciences, Kyushu University, Fukuoka, Japan (S.O.S., T.I.); Philips Electronics Japan, Tokyo, Japan (M.O., M.V.C.)

Corresponding Author: Osamu Togao, MD, PhD, Department of Clinical Radiology, Graduate School of Medical Science, Kyushu University, Fukuoka, Japan; 3-1-1 Maidashi Higashi-ku Fukuoka, Japan, 812-8582 (togao@radiol.med.kyushu-u.ac.jp).

Background. Our aim was to assess the diagnostic performance of intravoxel incoherent motion (IVIM) MR imaging for differentiating high-grade gliomas (HGGs) from low-grade gliomas (LGGs).

Methods. Forty-five patients with diffuse glioma (age 50.9 ± 20.4 y; 26 males, 19 females) were assessed with IVIM imaging using 13 *b*-values (0–1000 s/mm^2) at 3T. The perfusion fraction (*f*), true diffusion coefficient (*D*), and pseudo-diffusion coefficient (*D**) were calculated by fitting the bi-exponential model. The apparent diffusion coefficient (ADC) was obtained with 2 *b*-values (0 and 1000 s/mm^2). Relative cerebral blood volume was measured by the dynamic susceptibility contrast method. Two observers independently measured *D*, ADC, *D**, and *f*, and these measurements were compared between the LGG group ($n = 16$) and the HGG group ($n = 29$).

Results. Both *D* (1.26 ± 0.37 mm^2/s in LGG, 0.94 ± 0.19 mm^2/s in HGG; $P < .001$) and ADC (1.28 ± 0.35 mm^2/s in LGG, 1.03 ± 0.19 mm^2/s in HGG; $P < .01$) were lower in the HGG group. *D* was lower than ADC in the LGG ($P < .05$) and HGG groups ($P < .0001$). *D** was not different between the groups. The *f*-values were significantly larger in HGG (17.5 ± 6.3%) than in LGG (5.8 ± 3.8%; $P < .0001$) and correlated with relative cerebral blood volume ($r = 0.85$; $P < .0001$). Receiver operating characteristic analyses showed areas under curve of 0.95 with *f*, 0.78 with *D*, 0.73 with ADC, and 0.60 with *D**.

Conclusion. IVIM imaging is useful in differentiating HGGs from LGGs.

Keywords: diffusion, glioma, intravoxel incoherent motion, MRI, perfusion.

Gliomas are the most common primary neoplasms of the brain, varying histologically from low grade to high grade in World Health Organization (WHO) classification.[1] The differentiation between low-grade gliomas (LGGs; grade II) and high-grade gliomas (HGGs; grades III, IV) is critical, since the prognosis and thus the therapeutic strategy could differ substantially depending on the grade. Because of their dismal prognosis, HGGs are usually treated with surgical resection followed by adjuvant radiation therapy and chemotherapy.[2] HGGs misdiagnosed as LGGs will be treated less aggressively than necessary, and vice versa.

Many investigators have attempted to develop MR imaging biomarkers for the grading of gliomas: diffusion-weighted (DW) imaging,[3,4] perfusion-weighted (PW) imaging,[5–7] and proton MR spectroscopy[8,9] provide in vivo physiologic information for tumor characterization. These methods have been found to be of increasing utility in assessments of the grade of gliomas. Some studies showed that the apparent diffusion coefficient (ADC) measured by DW imaging had high diagnostic performance in differentiating HGGs from LGGs.[3,4] However, other studies showed a substantial overlap in the ADC values between LGGs and HGGs,[10] or no difference between them.[11]

A recent study showed that the combination of dynamic susceptibility contrast (DSC) PW imaging and DW imaging could significantly improve the diagnostic performance of the

Received 23 March 2015; accepted 10 June 2015

differentiation.[12] In clinical settings, the use of DSC PW imaging may frequently be limited because of the patient's age, renal dysfunction, high injection rate, and/or allergic reaction to the contrast material.

The grades of gliomas are histologically determined based on the presence of cellular anaplasia and nuclear atypia, cell density, mitoses, microvascular proliferation, and necrosis.[13] The diffusion property has been reported to reflect cell density, which is related to the active cell proliferation,[3,14,15] and the perfusion property is largely determined by the microvascular proliferation or angiogenesis of tumors. Both cell proliferation and angiogenesis are major features in determining the histological grades of gliomas. The preoperative imaging of diffuse gliomas with estimation of grade is important. There can be inherent sampling errors associated with intratumoral histological heterogeneity in gliomas. Inappropriate sampling from sites with lower histological grade in a tumor may lead to underestimation of the true grades. Thus, the preoperative grading may be helpful in planning and determining a surgical approach, either biopsy or partial or total resection. Moreover, a recent study revealed that relative cerebral blood volume (rCBV) measured by DSC PW imaging better predicted prognosis of patients of diffuse glioma,[16] indicating the superior performance of perfusion imaging over histopathology in predicting glioma outcome.

Le Bihan et al[17] developed a method to visualize microscopic motions of water. Their theory aimed to separate diffusion and perfusion parameters based on an intravoxel incoherent motion (IVIM) model using a single DW acquisition scheme. The ADC, which is frequently calculated with a pair of *b*-values (eg, 0 and 1000 s/mm^2), includes contributions from the microcirculation of blood in capillaries (perfusion) in in vivo tissues.[17] The ADC can be overestimated especially in tumors with high vascularity. The IVIM model applies bi-exponential fitting to signal decay obtained with multiple *b*-values and then separates true diffusion and capillary perfusion. In other words, IVIM MR imaging allows us to simultaneously obtain both diffusion and perfusion imaging. IVIM imaging has some clear theoretical advantages over DSC PW imaging and conventional DW imaging. First, it is not necessary to use contrast agents and a rapid intravenous injection with IVIM imaging as in DSC PW imaging. Second, IVIM exploits a relatively simple mathematical analysis, and there is no need to obtain the arterial input function or perform deconvolution and leakage correction. Third, the geometry for diffusion and perfusion imaging is identical in IVIM, since these parameters are obtained from the same data set. Fourth, the true diffusion coefficient (*D*) measured with IVIM imaging could reflect the diffusion status more accurately than ADC, since the influence of perfusion is excluded in the calculation of *D*. Finally, IVIM is inherently quantitative and does not need any corrections. To date, there have been only 2 studies that investigate the utility of IVIM imaging for glioma. Federau et al,[18] in their study involving 21 patients with glioma, reported that the *f*-value is higher in HGG than in LGG, but no difference was found in *D* or *D** between the groups. Bisdas et al,[19] in their study involving 22 patients with glioma, showed that the *f*-values and *D** values were higher in HGG than in LGG, but *D* was not different between the groups. The consensus for the usefulness of each IVIM-derived parameter has not been established yet. The purpose of this study was to prospectively evaluate the diagnostic performance of IVIM-derived parameters in differentiating HGGs from LGGs in a larger population of patients.

Materials and Methods

Patients

From January 2013 to May 2015, forty-five consecutive patients with diffuse glioma (age 50.9 ± 20.4 y; 26 males, 19 females) who underwent a subsequent surgical resection or biopsy were enrolled. Twenty-nine of the 45 patients underwent total resection, and 14 and 2 patients underwent partial resection/debulking and biopsy, respectively. The numbers of patients with grades II, III, and IV gliomas were 16, 6, and 23, respectively. Thus, the LGG group comprised 16 patients (age 37.1 ± 12.2 y; 10 males, 6 females) and the HGG group 29 patients (age 58.4 ± 20.1 y; 16 males, 13 females). The patients' histological types of gliomas were as follows: 10 diffuse astrocytomas, 5 oligodendrogliomas, 1 oligoastroctyoma, 1 anaplastic astrocytoma, 5 anaplastic oligoastrocytomas, and 23 glioblastoma multiforme (GBM). All tumors were located supratentorially. The interval between MRI and the surgery was shorter than 2 weeks in all patients. This prospective study was approved by our institutional review board, and informed consent was obtained.

Intravoxel Incoherent Motion MRI

IVIM imaging was performed on a 3T clinical scanner (Achieva TX, Philips Healthcare) with an 8-channel head coil. IVIM imaging was performed in axial planes by using a single-shot echo-planar imaging diffusion sequence, with 13 *b*-values (0, 10, 20, 30, 50, 80, 100, 200, 300, 400, 600, 800, 1000 s/mm^2) in 3 orthogonal directions. The other imaging parameters were: repetition time (TR) = 2500 ms; echo time (TE) = 70 ms; matrix = 128 × 126 (reconstructed to 256 × 256); slice thickness = 5 mm, field of view = 230 × 230 mm; number of slices = 11, sensitivity encoding factor 1.5; scan time = 2 min 7 s. For reference, several standard MR images were acquired, including T1-weighted, T2-weighted, fluid attenuation inversion recovery, and contrast-enhanced T1-weighted.

Intravoxel Incoherent Motion Data Analysis

The standard IVIM 2-compartment diffusion model was employed, with a capillary perfusion component and a nonvascular compartment.[17] Signal decay was estimated by using the following bi-exponential equation:

$$\frac{SI}{SI_0} = (1-f) \times \exp(-bD) + f \times \exp(-bD^*) \qquad (1)$$

where *D* and *D** are the true diffusion coefficient and the pseudo-diffusion coefficient, respectively; SI and SI_0 are the signal intensity at a given *b*-value and at *b* = 0 s/mm^2, respectively; and *f* is the volume fraction within a voxel of water flowing in perfused capillaries. The conventional ADC relies upon the contribution of both molecular diffusion from random thermic molecular motion (Brownian motion) and motion of water

molecules in blood related to perfusion through capillaries, both of which can be considered incoherent motion with respect to transverse magnetization because of the assumed randomness of microscopic water translation with both. It also relies upon the following: ADC = D if there is no active perfusion within a voxel, whereas ADC > D if there is perfusion within a voxel. The pseudo-diffusion coefficient D^* represents the incoherent molecular translation of water within flowing blood when that blood flow changes capillary segments several times during the TE and thereby mimics the random walk of the diffusion process.

The signal decay was fitted in a single step on a voxel-by-voxel basis to create each parameter map of D, D^*, and f by using an interactive data language–based software program (DWI TOOL R1.5, Philips Medical Systems). In addition, conventional ADC maps were created with 2 b-values ($b = 0$ and 1000 s/mm^2).

Dynamic Susceptibility Contrast Perfusion-Weighted MRI

After placement of an intravenous catheter in the antecubital fossa and 7 min prior to DSC PW imaging acquisition, 0.05 mmol/kg gadolinium contrast agent (gadopentetate dimeglumine or gadodiamide) was administered as a preload dose to minimize T1 leakage effects.[20] During the acquisition, an additional 0.05 mmol/kg bolus was administered at 5 mL/s. The DSC PW imaging was obtained with a gradient-echo echo-planar imaging sequence using the following parameters: TR = 1428 ms, TE = 35 ms, matrix = 288 × 288, slice thickness = 5 mm, field of view = 230 × 230 mm, number of slices = 22, sensitivity encoding factor 2, scan time = 1 min 26 s.

Relative CBV maps were generated using an Osirix workstation (version 5.0.2, 64 bit; http://www.osirix-viewer.com/) with IB Neuro software (v1; Imaging Biometrics) to calculate the whole-brain CBV from the DSC PW imaging data.[21] Briefly, after excluding the first 4 time points of each DSC PW imaging data set due to saturation effects, signal intensities were normalized to baseline and then converted to the change in relaxivity over time [$\Delta R2^*(t)$] for the entire brain. The CBV was calculated voxel-by-voxel by integrating the area under the $\Delta R2^*(t)$ curve, ending at the time point 40 s after the nadir signal intensity of the first-pass bolus. All CBV values were corrected for T1-weighted leakage with preload dosing, and a modeling algorithm was used to correct T2/T2*-weighted residual effects.[22] The CBV maps were normalized to contralateral normal-appearing white matter (NAWM) to create rCBV maps. DSC PW imaging was not performed in 3 of the 45 patients because of age (6 y, $n = 1$) and poor health condition ($n = 2$).

Regions of Interest

Two experienced neuroradiologists (O.T. and K.Y. with 15 and 13 y of experience, respectively) carefully placed 3 circular regions of interest (ROIs, ~0.26 cm^2, 32 pixels) using an ImageJ plugin (v1.43u; National Institutes of Health) in the solid component of a tumor to include the area with the minimum D or maximum f-value, and the best effort was given to avoid cystic, necrotic, and hemorrhagic components of the tumor with reference to conventional MR images (Supplementary Fig. 1).[23–25]

The ADCs were measured with the same ROIs for the minimum D values, and the D^* values were measured in the same ROIs for the maximum f-values. The measured values in the 6 ROIs by the 2 observers were then averaged to represent each tumor. D, ADC, and f were also measured in a larger circular ROI (~1.8 cm^2, 200 pixels) placed in NAWM. Similarly, we also measured the rCBV in 3 ROIs (~0.30 cm^2, 44 pixels) with maximum values in the tumor as well as in a larger ROI (~1.8 cm^2, 264 pixels) placed in NAWM.

Histopathological Evaluation

The histopathological diagnosis was determined with resected specimens according to the WHO criteria by 2 established neuropathologists (S.O.S. and T.I., with 22 and 31 y of experience, respectively). Tissue samples obtained from the specimens were routinely processed and stained for hematoxylin and eosin (H&E), and stained immunohistochemically for CD31.

Statistical Analysis

All values are expressed as mean ± SD. Interobserver agreement for each parameter from the 2 observers was analyzed by calculating the intraclass correlation coefficient (ICC), Pearson correlation, and Bland–Altman plot. ICCs are considered to be excellent when >0.74.[26] D, ADC, D^*, and f-values were compared between the LGG and HGG groups by unpaired t-test. D and ADC were compared within the LGG and HGG groups by paired t-test.

The relationship between f and rCBV was evaluated with Pearson correlation. We used a receiver operating characteristic (ROC) analysis to evaluate the diagnostic accuracy of D, ADC, D^*, and f in differentiating LGGs from HGGs. We considered area under the curve (AUC) values <0.7, 0.7–0.9, and >0.9 to indicate low, medium, and high diagnostic performance, respectively. Statistical analyses were performed with commercially available software packages (SPSS; Prism GraphPad 5.0; and MedCalc v13.1.2.0). $P < .05$ was considered significant.

Results

The Signal Decay Curves of Low-Grade and High-Grade Gliomas

The signal intensity of the tumor bi-exponentially decayed as a function of the b-value in both LGGs and HGGs. The goodness of fit (R^2) was above 0.997 in all cases. However, the signal decay curves were different between the LGGs and HGGs, suggesting that they have characteristic IVIM parameters (Supplementary Fig. 2).

Interobserver Agreement

Our evaluation of the interobserver agreement for D and the f-values of the tumors in the 45 patients showed excellent agreement, with an ICC of 0.90 and r of 0.83 ($P < .0001$) for D, an ICC of 0.88 and r of 0.79 ($P < .0001$) for ADC, an ICC of 0.95 and r of 0.92 ($P < .0001$) for D^*, and an ICC of 0.94 and r of 0.91 ($P < .0001$) for the f-values. Bland–Altman plot analysis showed excellent accordance of measurements by the 2

observers, with only 2 values for *D* and ADC and 3 values for *D** and *f* beyond the 95% limits of agreement (Supplementary Fig. 3).

Intravoxel Incoherent Motion Parameters in Each WHO Grade and Histology

Table 1 summarizes the measured parameters for each WHO grade and histology. The *D*-values of grade III ($P < .05$) and grade IV ($P < .01$) gliomas were significantly lower than those of the grade II gliomas. The ADCs of the grade III ($P < .05$) and grade IV ($P < .05$) gliomas were significantly lower than those of the grade II gliomas. *D** did not differ among the grades. The *f*-values of the grade III ($P < .001$) and grade IV ($P < .001$) gliomas were significantly higher than those of the grade II gliomas. *D*, ADC, and the *f*-values in NAWM were $0.74 \pm 0.06 \times 10^{-3}$ mm^2/s, $0.78 \pm 0.06 \times 10^{-3}$ mm^2/s, and 5.3% ± 1.5%, respectively. The rCBVs of the grade III ($P < .01$) and grade IV ($P < .001$) gliomas were significantly higher than those of the grade II gliomas.

Differentiation of LGG and HGG Using IVIM Parameters

When we grouped the grades III and IV tumors ($n = 29$) as the HGG group and compared them with the LGG group (grade II, $n = 16$), we observed significant differences between the groups in *D* ($1.26 \pm 0.37 \times 10^{-3}$ mm^2/s in LGG and $0.94 \pm 0.19 \times 10^{-3}$ mm^2/s in HGG, $P < .001$) and ADC ($1.28 \pm 0.35 \times 10^{-3}$ mm^2/s in LGG and $1.03 \pm 0.19 \times 10^{-3}$ mm^2/s in HGG, $P < .01$) (Fig. 1A). *D** showed wide variability, and no difference was found between the groups (Fig. 1B). There was a significant difference between the groups in *f*-value (5.8% ± 3.8% in LGG and 17.5% ± 6.3% in HGG, $P < .0001$) (Fig. 1C).

The diagnostic performance of each parameter in differentiating HGG from LGG is shown in Table 2 and Fig. 1D. The results of the ROC analysis for discriminating HGG from LGG demonstrated that the *f*-values showed the highest diagnostic performance, with AUC values of 0.95. *D* and ADC showed moderate diagnostic performance, with AUC values of 0.78 and 0.73, respectively. *D** showed low diagnostic performance in this discrimination. Relative CBV showed the equivalent diagnostic performance to the *f*-values.

Figures 2 and 3 and Supplementary Fig. 4 show representative cases of grade II (diffuse astrocytoma), grade III (anaplastic astrocytoma), and grade IV (GBM), respectively. Lower *D* and ADC and higher *f*-values and rCBV were observed in grade III and grade IV compared with grade II glioma.

Comparison of the D *and ADC Values*

D was significantly lower than ADC in LGG ($P < .05$) and in HGG ($P < .0001$; Fig. 1A). There were 2.7% ± 4.2% and 10.0% ± 5.4% differences between *D* and ADC in LGG and HGG, respectively.

Correlation Between the f*- and rCBV Values*

There was a strong positive correlation between the *f*- and rCBV values in the tumor ROIs ($P < .0001$, $r = 0.85$; Fig. 4). Significant correlations between the *f*- and rCBV values were also found

Table 1. Measurements in each WHO grade and histology

	Histology	*n*	*D* ($\times 10^{-3}$ mm^2/s)		ADC ($\times 10^{-3}$ mm^2/s)		*D** ($\times 10^{-3}$ mm^2/s)		*f*, %	
Grade II ($n = 16$)	Astrocytoma	10	1.37 ± 0.35	1.26 ± 0.37	1.39 ± 0.32	1.28 ± 0.35	11.25 ± 11.65	12.07 ± 9.74	5.9 ± 4.2	5.8 ± 3.8
	Oligodendroglioma	5	0.95 ± 0.26		0.98 ± 0.26		14.93 ± 6.47		6.1 ± 3.9	
	Oligoastrocytoma	1	1.60		1.61		16.06		3.9	
Grade III ($n = 6$)	Anaplastic astrocytoma	1	1.01	0.87 ± 0.19*	1.09	0.96 ± 0.22*	26.39	11.49 ± 9.11	12.7	18.9 ± 7.7***
	Anaplastic oligoastrocytoma	5	0.84 ± 0.20		0.94 ± 0.24		8.52 ± 6.09		20.1 ± 7.9	
Grade IV ($n = 23$)	GBM	23	0.96 ± 0.19**		1.05 ± 0.19*		15.18 ± 8.84		17.1 ± 6.0***	
	Histology	*n*	rCBV							
Grade II ($n = 16$)	Astrocytoma	10	2.4 ± 2.8	2.4 ± 2.4						
	Oligodendroglioma	5	2.6 ± 1.8							
	Oligoastrocytoma	1	1.4							
Grade III ($n = 6$)	Anaplastic astrocytoma	1	7.0	10.4 ± 4.6**						
	Anaplastic oligoastrocytoma	5	11.1 ± 4.8							
Grade IV ($n = 23$)	GBM	23	9.9 ± 5.7***							

Note: All values are the averages of the measurements by the 2 observers.
*$P < .05$, **$P < .01$, ***$P < .001$ compared with grade II.

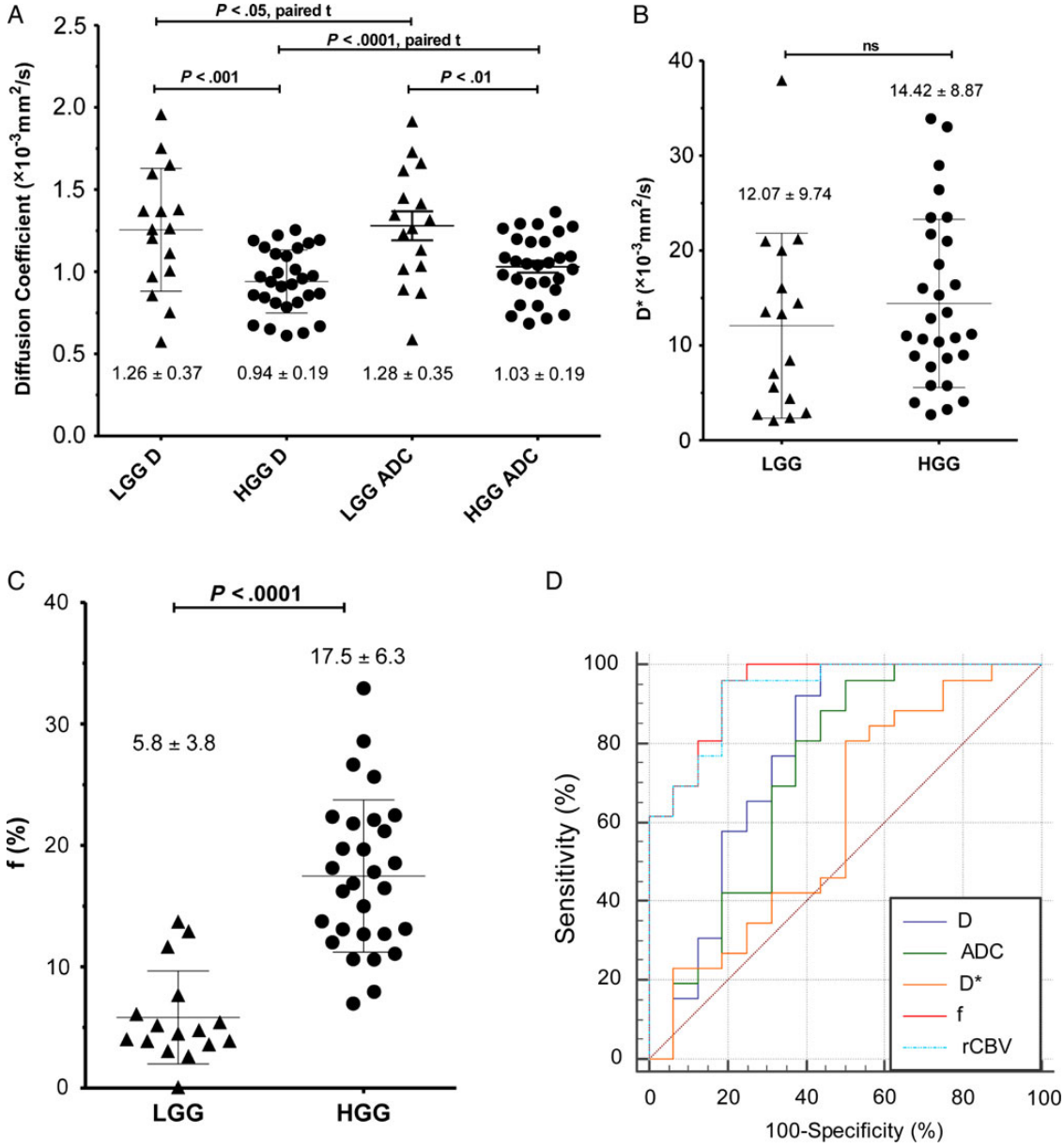

Fig. 1. (A) *D* and ADC values in LGGs (grade II) and HGGs (grades III and IV). Significant differences were seen between the groups in *D* and ADC. The *D* is significantly lower than ADC in the LGG and HGG groups. (B) *D** in the LGGs and HGGs. The *D**-values are not significantly different between the groups. (C) The *f*-value in the LGGs and HGGs. The *f*-values of the HGG group were significantly higher than those of the LGG group. (D) ROC analysis for discriminating HGGs from LGGs. The *f*-value showed the highest diagnostic performance, with AUC = 0.95, which was equivalent to that of rCBV (0.93). *D* and ADC showed moderate diagnostic performance, with AUCs = 0.78 and 0.73, respectively. *D** showed the low diagnostic performance, with AUC = 0.60.

within the LGG group ($P < .0001$, $r = 0.88$) as well as the HGG group ($P < .0001$, $r = 0.71$).

Histopathological Evaluation

H&E staining showed that cell density increased as the glioma grade advanced (Figs 2E and 3E, Supplementary Fig. 4E). Immunohistochemical staining for CD31 revealed that the number of blood vessels increased with the grade (Figs 2F and 3F, Supplementary Fig. 4F). GBM showed high cell density, nuclear anaplasia, mitoses, and microvascular proliferation characterized by glomeruloid blood vessels (Supplementary Fig. 4E–F).

Discussion

The results of the present study elucidated that both the diffusion and perfusion parameters of IVIM imaging are useful for

Table 2. Diagnostic performance of parameters in differentiating HGG from LGG

Parameters	Cutoff Value	Sensitivity, %	Specificity, %	AUC
D	$\leq 1.25 \times 10^{-3}$ mm^2/s	100	56.2	0.78
ADC	$\leq 1.29 \times 10^{-3}$ mm^2/s	96.6	50.0	0.73
*D**	$\geq 8.43 \times 10^{-3}$ mm^2/s	75.9	50.0	0.60
f	≥7.7%	96.6	81.2	0.95
rCBV	≥2.24	96.2	81.2	0.93

differentiating HGGs from LGGs. Regarding diffusion parameters, we found that both *D* and ADC provided good sensitivity and moderate specificity in this differentiation. Diffusion parameters reflect water molecule movement (ie, Brownian motion), which is restricted in biological conditions. ADC has been reported to demonstrate sensitivity to cell density.[14,15,27] Dense cells provide more restriction of water movement, presumably because of increased cell membranes and fraction of intracellular space. Accordingly, ADC measurement has been implemented for the assessment of cell density in many types of tumors.

Cellularity and mitotic activity are important criteria in the histopathological grading of gliomas. Many studies reported that the ADC calculated with a pair of *b*-values (0 and 1000 s/mm^2) decreased with the glioma grade. For example, in their series of 162 diffuse gliomas, Hilario et al[12] reported a significant difference in the ADC value for differentiating HGGs from LGGs ($P < .001$). The ADC cutoff value of 1.185×10^{-3} mm^2/s generated the best combination of sensitivity (97.6%) and specificity (53.1%). Similar findings were reported by Lee et al,[28] Kim et al,[29] and Arvinda et al.[23] Our ADC results are well consistent with these previous studies.

However, we demonstrated that the *D* value was significantly lower than ADC in the LGG group ($P < .05$) and the HGG group ($P < .0001$), and there was a difference of ~10% between the *D* and ADC values in HGG. This difference between *D* and ADC in HGG is most likely due to the increased perfusion fraction in HGG. The *D* value showed better sensitivity and thus diagnostic performance in the differentiation between LGGs and HGGs. Although the ADC that we calculated from the pair of *b*-values had adequate diagnostic performance in this differentiation, it is worth keeping in mind that there is still room for improvement using *D* values calculated from the IVIM model instead of conventional ADC measurements. The usefulness of *D* and ADC found in this study was not observed in the previous IVIM studies of gliomas where the numbers of patients were small.[18,19]

High vascularity is another important criterion in the histopathological grading of gliomas, since the malignant process of gliomas is characterized by neoangiogenesis. The histopathological assessments in our study revealed that the number of blood vessels increased with the progression of glioma grade. In particular, glomeruloid microvascular proliferation was observed in GBM. Glioma cells associate with both existing and newly generated blood vessels at different stages of the disease. At the early stage, existing vessels serve as a pathway for tumor invasion.[30] At a later stage, new vessels are generated through angiogenesis. Watkins et al[31] revealed that glioma cells populate the perivascular space of preexisting vessels and displace astrocytic endfeet from endothelial or vascular smooth muscle cell. This results in the loss of astrocyte-mediated gliovascular coupling and the control over regulation of vascular tone. In the Watkins study, most glioma cells associated with capillaries (<7 μm diameter) and about one third of the cells were attached to penetrating arterioles or collecting veins (7–35 μm diameter).[31] These facts indicated that perfusion fraction measured with IVIM imaging included not only capillary developed by angiogenesis but also preexisting small arterioles or collection veins in which regulation of vascular tone was impaired. The *f*-values were larger in HGG than in LGG, which is consistent with the previous 2 IVIM studies.[18,19] To date, many researchers have used DSC PW imaging or more recently an arterial spin labeling technique for grading gliomas. In the previous studies, the rCBV measurements by DSC PW imaging correlated with the glioma grades and histological findings of increased vascularity of gliomas. Hilario et al[12] reported that the rCBV in HGGs (6.85) was significantly higher than that in LGGs (2.36, $P < .01$). Similar findings were reported in other studies: the rCBV values for LGGs and HGGs were 1.69 and 6.40[32] and 2.14 and 5.18,[33] respectively. We found that the *f*-value in the present HGGs was ~3 times higher than that in the LGG group, and this difference was significant. In addition, the *f*-values measured with IVIM imaging strongly correlated with the rCBV obtained with DSC PW imaging. Interestingly, a strong correlation was found not only in all samples but also in the LGG group and the HGG group. These results suggest that the *f*-value is a reliable quantitative parameter to evaluate the vascularity of gliomas and has diagnostic ability equivalent to that of rCBV with DSC PW imaging. It should be noted that *f* is a quantitative value obtained with direct measurement in the tumors, without any normalization with a measure in the contralateral NAWM, as is currently performed with DSC PW imaging because of its poor quantitative ability.

In the present study, the *f*-value showed the best diagnostic performance among all parameters, indicating that the *f*-value has an additive value to ADC or *D* in the differentiation of LGGs and HGGs. Moreover, the *f*-value showed equivalent diagnostic performance to the rCBV. These results are in line with the several studies that revealed the added value of PW imaging to DW imaging for the more accurate diagnosis of glioma grades.[12,29] IVIM imaging can simultaneously provide both diffusion and perfusion information in the same geometry, which could be an advantage over DSC PW imaging, as already mentioned.

In IVIM imaging, it is assumed that blood protons stay in the capillary network during the measurement time.[17] An exchange between extra- and intracapillary water may be a source of mistakes in the evaluation of *f*-values. Since it has been reported that vascular permeability increases with the grades of glioma,[34] this could have affected the measurements of *f*-values in the present study to some extent. The IVIM model assumes that the flowing component (*f*) and the static component (1 – *f*) have similar T2 relaxation times. If this is not true, the *f*-value can be influenced by the difference in T2 between the 2 components.[17] In the present study, we did not take T2 relaxation times into account in the IVIM analysis. Apparently, the T2 of tissues in many disease statuses including gliomas is prolonged. The *f*-value measured in T2-prolonged tissue will

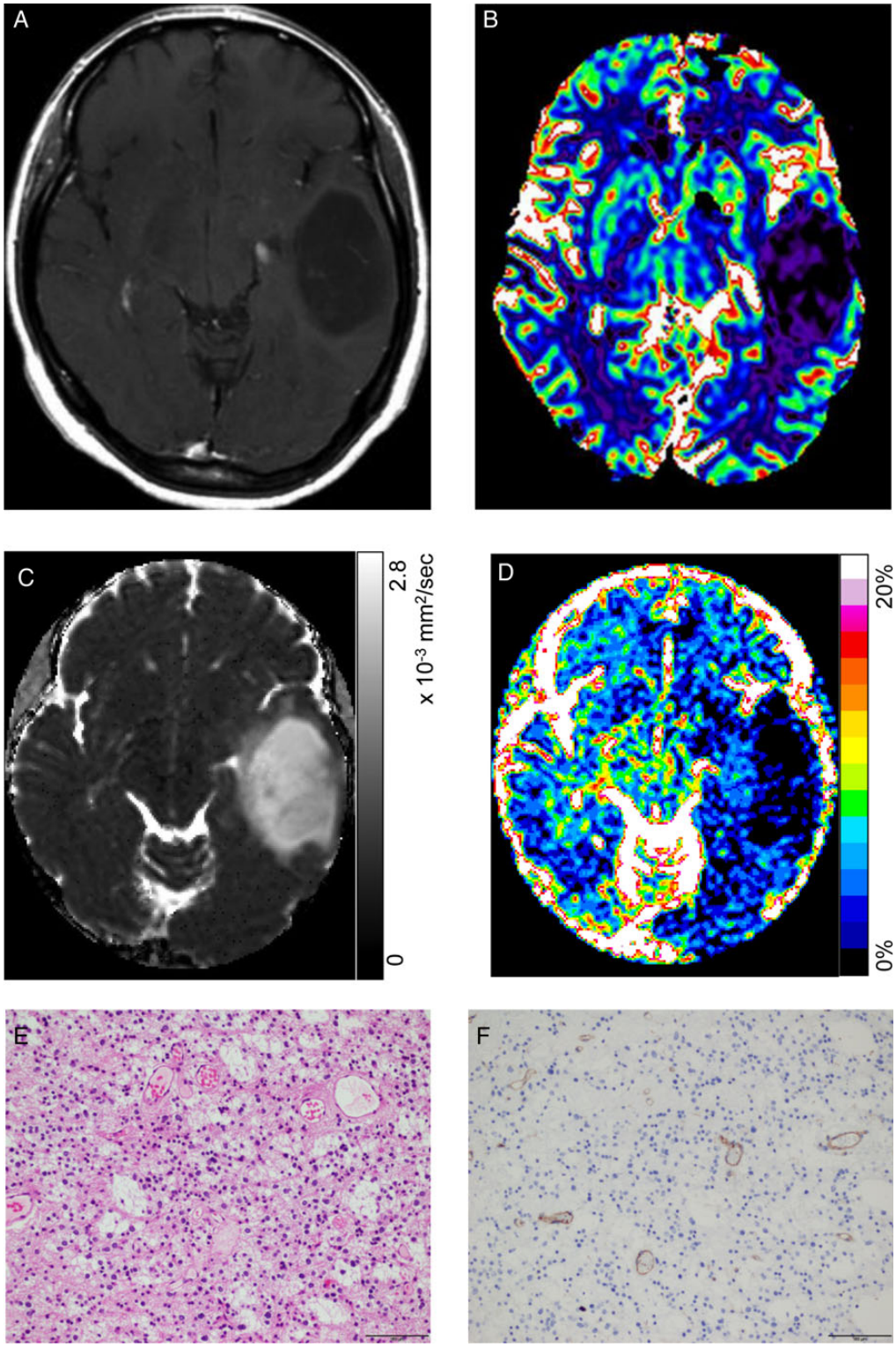

Fig. 2. Images obtained in a 39-year-old woman with a diffuse astrocytoma (WHO grade II). (A) A contrast-enhanced transverse T1-weighted image shows faint enhancement in the tumor. (B) The rCBV map shows decreased rCBV (0.5) in the lesion. (C) The *D* map shows an increased *D* value (1.75×10^{-3} mm^2/s) in the lesion compared with the cutoff value (1.25×10^{-3} mm^2/s). (D) The *f* map shows a decreased *f*-value (3.1%) in the lesion compared with the cutoff value (7.7%). (E) H&E staining shows relatively low cell density with microcytic and mucinous background. (F) Immunohistochemical staining for CD31 shows the small number of blood vessels. Bars = 100 μm.

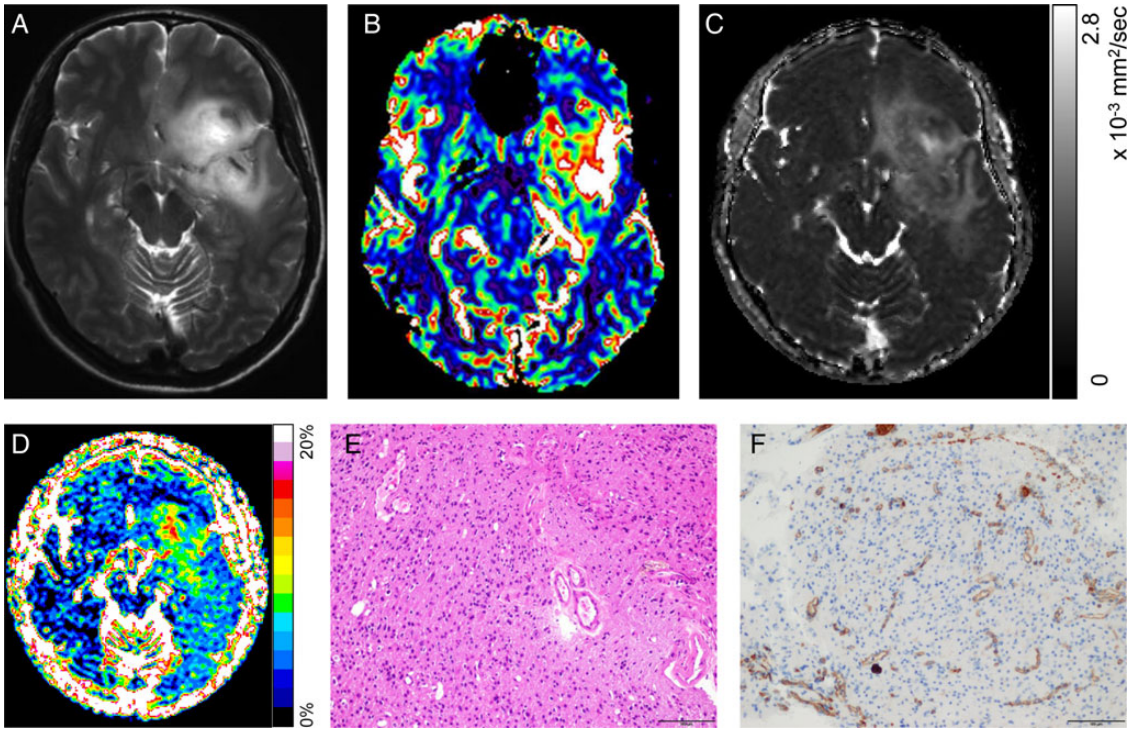

Fig. 3. Images obtained in a 38-year-old man with an anaplastic astrocytoma (WHO grade III). (A) A transverse T2-weighted image shows a heterogeneous hyperintense lesion in the left frontotemporal lobe. No contrast enhancement was observed in the tumor (not shown). (B) The rCBV map shows increased rCBV (7.0) in the lesion. (C) The *D* map shows a slightly lower *D* value (1.10×10^{-3} mm^2/s) in the lesion compared with the cutoff value (1.25×10^{-3} mm^2/s). (D) The *f* map shows an increased *f*-value (12.7%) in the lesion compared with the cutoff value (7.7%). (E) H&E staining shows relatively moderate cell density. (F) Immunohistochemical staining for CD31 shows the increased number of blood vessels compared with grade II glioma. Bars = 100 μm.

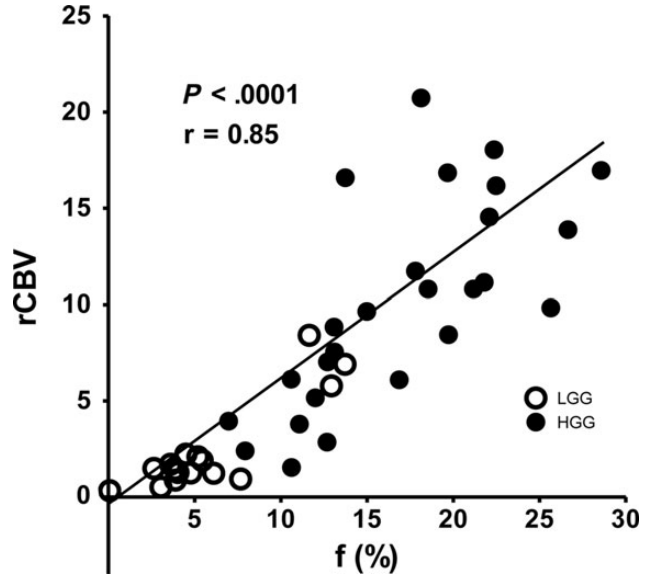

Fig. 4. Correlation between *f* and rCBV in the tumors. A strong positive correlation was observed between these 2 parameters.

show an underestimation of its value. This should be borne in mind, since gliomas can express increased variability with the elevation of their grade and thus present variable T2 values.

Another IVIM-derived parameter, *D**, was not useful in the differentiation in this study because we could not obtain stable values in both the LGG and HGG groups. Previous studies suggested that *D** was less reproducible[35] and could be strongly affected by the cardiac cycle.[36] It is desirable to develop a reliable method to quantify *D** in tumors.

Our results demonstrated the possibility that IVIM imaging is an alternative method to DSC PW imaging in evaluating vascularity of diffuse gliomas. However, more studies are necessary to investigate consistencies and discrepancies of the 2 different approaches. To perform such comparisons, it is desirable to establish optimal imaging acquisition parameters and analysis methods for each technique. Although DSC PW imaging has been the most commonly used method to assess cerebral perfusion, this technique greatly depends on many factors, including the dose or injection rate of contrast agent, imaging sequence and acquisition parameters, and postprocessing and interpretation of data.[37] The quantitative ability of IVIM imaging could also be affected by imaging parameters, especially for the selection and number of *b*-values, and the way of fitting. The correction for T2 differences among tissues should be incorporated to perform more accurate quantifications. Establishment of optimal imaging conditions allows us to perform head-to-head comparisons of IVIM and DSC PW imaging in future studies. Other potential future directions of IVIM imaging studies are to investigate whether the combination of various IVIM-derived parameters improves accuracy in grading gliomas

and whether IVIM imaging can be used to monitor therapeutic response and treatment effects, including the differentiation of pseudoprogression from true progression, and radiation-induced necrosis and tumor recurrence after treatment.

The strengths of the present study include its prospective design, the short interval between imaging and surgery (<2 wk), and the complete histopathology-based diagnosis in all patients. However, there were study limitations. First, the cohort is relatively small, especially that of grade III glioma ($n = 6$). This could be the reason why we did not observe significant differences in some comparisons between grades II and III or between grades III and IV. Second, the placement of ROIs was subjective. To overcome this issue, the 2 experienced neuroradiologists acted independently, and the agreement of the measurements was strictly evaluated with 3 types of statistical tests; however, the generalizability of our results may be limited by the fact that the accuracies in determining glioma grade were based on the averaging of the parameter values measured by 2 observers instead of one, particularly if this were to be used in the clinic. Third, our results could be specific to the method of small and select ROI placement, although this method has been used in previous studies.[23–25] Automatic segmentation of tumor area combined with histogram analysis could overcome this issue.

In conclusion, IVIM imaging can be used as a noninvasive quantitative imaging method in differentiating HGGs from LGGs. This method simultaneously provided both diffusion and perfusion parameters, which are related to the essential histological features in gliomas. All parameters but D^* were useful for the differentiation. Among them, the *f*-value showed the best diagnostic performance, which was equivalent to that of DSC PW imaging. Although both *D* and ADC showed moderate performance, *D* improved diagnostic ability compared with ADC. Its further use can contribute to diagnosis and treatment planning for patients with gliomas.

Funding

This work was supported by grants-in-aid for Scientific Research numbers 80546565, 26461827, and 40322747, Japan.

Conflict of interest statement. Makoto Obara and Marc Van Cauteren are employees of Philips Electronics Japan.

References

1. Daumas-Duport C, Scheithauer B, O'Fallon J, et al. Grading of astrocytomas. A simple and reproducible method. *Cancer*. 1988; 62(10):2152–2165.
2. Law M, Yang S, Babb JS, et al. Comparison of cerebral blood volume and vascular permeability from dynamic susceptibility contrast-enhanced perfusion MR imaging with glioma grade. *AJNR Am J Neuroradiol*. 2004;25(5):746–755.
3. Sugahara T, Korogi Y, Kochi M, et al. Usefulness of diffusion-weighted MRI with echo-planar technique in the evaluation of cellularity in gliomas. *J Magn Reson Imaging*. 1999;9(1):53–60.
4. Bulakbasi N, Guvenc I, Onguru O, et al. The added value of the apparent diffusion coefficient calculation to magnetic resonance imaging in the differentiation and grading of malignant brain tumors. *J Comput Assist Tomogr*. 2004;28(6):735–746.
5. Aronen HJ, Gazit IE, Louis DN, et al. Cerebral blood volume maps of gliomas: comparison with tumor grade and histologic findings. *Radiology*. 1994;191(1):41–51.
6. Sugahara T, Korogi Y, Kochi M, et al. Correlation of MR imaging–determined cerebral blood volume maps with histologic and angiographic determination of vascularity of gliomas. *AJR Am J Roentgenol*. 1998;171(6):1479–1486.
7. Shin JH, Lee HK, Kwun BD, et al. Using relative cerebral blood flow and volume to evaluate the histopathologic grade of cerebral gliomas: preliminary results. *AJR Am J Roentgenol*. 2002;179(3):783–789.
8. Kaminogo M, Ishimaru H, Morikawa M, et al. Diagnostic potential of short echo time MR spectroscopy of gliomas with single-voxel and point-resolved spatially localised proton spectroscopy of brain. *Neuroradiology*. 2001;43(5):353–363.
9. Dowling C, Bollen AW, Noworolski SM, et al. Preoperative proton MR spectroscopic imaging of brain tumors: correlation with histopathologic analysis of resection specimens. *AJNR Am J Neuroradiol*. 2001;22(4):604–612.
10. Server A, Kulle B, Gadmar OB, et al. Measurements of diagnostic examination performance using quantitative apparent diffusion coefficient and proton MR spectroscopic imaging in the preoperative evaluation of tumor grade in cerebral gliomas. *Eur J Radiol*. 2011;80(2):462–470.
11. Lam WW, Poon WS, Metreweli C. Diffusion MR imaging in glioma: does it have any role in the pre-operation determination of grading of glioma? *Clin Radiol*. 2002;57(3):219–225.
12. Hilario A, Ramos A, Perez-Nunez A, et al. The added value of apparent diffusion coefficient to cerebral blood volume in the preoperative grading of diffuse gliomas. *AJNR Am J Neuroradiol*. 2012;33(4):701–707.
13. Louis DN, Ohgaki H, Wiestler OD, et al. The 2007 WHO classification of tumours of the central nervous system. *Acta Neuropathol*. 2007;114(2):97–109.
14. Lyng H, Haraldseth O, Rofstad EK. Measurement of cell density and necrotic fraction in human melanoma xenografts by diffusion weighted magnetic resonance imaging. *Magn Reson Med*. 2000; 43(6):828–836.
15. Chen L, Liu M, Bao J, et al. The correlation between apparent diffusion coefficient and tumor cellularity in patients: a meta-analysis. *PLoS One*. 2013;8(11):e79008.
16. Hilario A, Sepulveda JM, Perez-Nunez A, et al. A prognostic model based on preoperative MRI predicts overall survival in patients with diffuse gliomas. *AJNR Am J Neuroradiol*. 2014;35(6): 1096–1102.
17. Le Bihan D, Breton E, Lallemand D, et al. Separation of diffusion and perfusion in intravoxel incoherent motion MR imaging. *Radiology*. 1988;168(2):497–505.
18. Federau C, Meuli R, O'Brien K, et al. Perfusion measurement in brain gliomas with intravoxel incoherent motion MRI. *AJNR Am J Neuroradiol*. 2014;35(2):256–262.
19. Bisdas S, Koh TS, Roder C, et al. Intravoxel incoherent motion diffusion-weighted MR imaging of gliomas: feasibility of the method and initial results. *Neuroradiology*. 2013;55(10):1189–1196.
20. Boxerman JL, Schmainda KM, Weisskoff RM. Relative cerebral blood volume maps corrected for contrast agent extravasation significantly correlate with glioma tumor grade, whereas uncorrected maps do not. *AJNR Am J Neuroradiol*. 2006;27(4): 859–867.

21. Hu LS, Eschbacher JM, Heiserman JE, et al. Reevaluating the imaging definition of tumor progression: perfusion MRI quantifies recurrent glioblastoma tumor fraction, pseudoprogression, and radiation necrosis to predict survival. *Neuro Oncol*. 2012;14(7):919–930.
22. Paulson ES, Schmainda KM. Comparison of dynamic susceptibility-weighted contrast-enhanced MR methods: recommendations for measuring relative cerebral blood volume in brain tumors. *Radiology*. 2008;249(2):601–613.
23. Arvinda HR, Kesavadas C, Sarma PS, et al. Glioma grading: sensitivity, specificity, positive and negative predictive values of diffusion and perfusion imaging. *J Neurooncol*. 2009;94(1):87–96.
24. Higano S, Yun X, Kumabe T, et al. Malignant astrocytic tumors: clinical importance of apparent diffusion coefficient in prediction of grade and prognosis. *Radiology*. 2006;241(3):839–846.
25. Togao O, Yoshiura T, Keupp J, et al. Amide proton transfer imaging of adult diffuse gliomas: correlation with histopathological grades. *Neuro Oncol*. 2014;16(3):441–448.
26. Shrout PE, Fleiss JL. Intraclass correlations: uses in assessing rater reliability. *Psychol Bull*. 1979;86(2):420–428.
27. Togao O, Doi S, Kuro-o M, et al. Assessment of renal fibrosis with diffusion-weighted MR imaging: study with murine model of unilateral ureteral obstruction. *Radiology*. 2010;255(3):772–780.
28. Lee EJ, Lee SK, Agid R, et al. Preoperative grading of presumptive low-grade astrocytomas on MR imaging: diagnostic value of minimum apparent diffusion coefficient. *AJNR Am J Neuroradiol*. 2008;29(10):1872–1877.
29. Kim HS, Kim SY. A prospective study on the added value of pulsed arterial spin-labeling and apparent diffusion coefficients in the grading of gliomas. *AJNR Am J Neuroradiol*. 2007;28(9):1693–1699.
30. Winkler F, Kienast Y, Fuhrmann M, et al. Imaging glioma cell invasion in vivo reveals mechanisms of dissemination and peritumoral angiogenesis. *Glia*. 2009;57(12):1306–1315.
31. Watkins S, Robel S, Kimbrough IF, et al. Disruption of astrocyte-vascular coupling and the blood–brain barrier by invading glioma cells. *Nat Commun*. 2014;5:4196.
32. Hakyemez B, Erdogan C, Ercan I, et al. High-grade and low-grade gliomas: differentiation by using perfusion MR imaging. *Clin Radiol*. 2005;60(4):493–502.
33. Law M, Yang S, Wang H, et al. Glioma grading: sensitivity, specificity, and predictive values of perfusion MR imaging and proton MR spectroscopic imaging compared with conventional MR imaging. *AJNR Am J Neuroradiol*. 2003;24(10):1989–1998.
34. Roberts HC, Roberts TP, Brasch RC, et al. Quantitative measurement of microvascular permeability in human brain tumors achieved using dynamic contrast-enhanced MR imaging: correlation with histologic grade. *AJNR Am J Neuroradiol*. 2000; 21(5):891–899.
35. Andreou A, Koh DM, Collins DJ, et al. Measurement reproducibility of perfusion fraction and pseudodiffusion coefficient derived by intravoxel incoherent motion diffusion-weighted MR imaging in normal liver and metastases. *Eur Radiol*. 2013; 23(2):428–434.
36. Federau C, Hagmann P, Maeder P, et al. Dependence of brain intravoxel incoherent motion perfusion parameters on the cardiac cycle. *PLoS One*. 2013;8(8):e72856.
37. Willats L, Calamante F. The 39 steps: evading error and deciphering the secrets for accurate dynamic susceptibility contrast MRI. *NMR Biomed*. 2013;26(8):913–931.